

Cite this: *Lab Chip*, 2011, **11**, 1262

www.rsc.org/loc

PAPER

## Waveguide confined Raman spectroscopy for microfluidic interrogation†

Praveen C. Ashok,\* Gajendra P. Singh, Helen A. Rendall, Thomas F. Krauss and Kishan Dholakia

Received 30th September 2010, Accepted 6th December 2010

DOI: 10.1039/c0lc00462f

We report the first implementation of the fiber based microfluidic Raman spectroscopic detection scheme, which can be scaled down to micrometre dimensions, allowing it to be combined with other microfluidic functional devices. This novel Raman spectroscopic detection scheme, which we termed as *Waveguide Confined Raman Spectroscopy* (WCRS), is achieved through embedding fibers on-chip in a geometry that confines the Raman excitation and collection region which ensures maximum Raman signal collection. This results in a microfluidic chip with completely alignment-free Raman spectroscopic detection scheme, which does not give any background from the substrate of the chip. These features allow a WCRS based microfluidic chip to be fabricated in polydimethylsiloxane (PDMS) which is a relatively cheap material but has inherent Raman signatures in fingerprint region. The effects of length, collection angle, and fiber core size on the collection efficiency and fluorescence background of WCRS were investigated. The ability of the device to predict the concentration was studied using urea as a model analyte. A major advantage of WCRS is its scalability that allows it to be combined with many existing microfluidic functional devices. The applicability of WCRS is demonstrated through two microfluidic applications: reaction monitoring in a microreactor and detection of analyte in a microdroplet based microfluidic system. The WCRS approach may lead to wider use of Raman spectroscopy based detection in microfluidics, and the development of portable, alignment-free microfluidic devices.

### Introduction

Optofluidic devices where optical detection techniques are incorporated into microfluidics and nanofluidics have played a crucial role in the advancement of Lab on a Chip technology.<sup>1</sup> In the field of bio-chemical analytics for qualitative and quantitative analyses of samples, microfluidics devices, combined with spectroscopic techniques have found a variety of applications.

Raman spectroscopy is a powerful analytical tool which is receiving attention from the microfluidic community as a viable detection technique owing to its high chemical specificity and high information content. One of the main advantages of Raman spectroscopy over other spectroscopic methods is its ability to achieve multi-component detection in an analyte as each component would exhibit its own fingerprint bands in the acquired Raman spectrum. Hence it is possible to achieve simultaneous monitoring of multiple analyte components in a microfluidic channel.

Microfluidic Raman spectroscopy (MRS), where Raman spectroscopy is used as a detection technique on a microfluidic platform, has been used for a variety of chemical and biological applications ranging from basic analyte detection to reaction

monitoring in a microreactor.<sup>2–8</sup> Its applications are still limited, when compared to other methods such as fluorescence spectroscopy or absorption spectroscopy.<sup>9</sup> The main hindrance has been the inherently low cross-section of the Raman scattering process. Also, in many cases, the weak Raman signal is overwhelmed by a strong spectral background arising from the substrate of the microfluidic chip. Hence, for the successful implementation of MRS, it is essential to ensure maximum collection efficiency and minimum interference of the background from the substrate.

In fact, the implementation of MRS has largely been restricted to free space, bulk optic geometries and, to the best of our knowledge, a genuine on-chip implementation has not been reported before. Bulk optic based Raman detection systems have two inherent limitations: background from the substrate and the lack of portability. A detailed discussion on the former issue can be found in some recent publications.<sup>6,10</sup> The other limitation of a bulk optic based system is its lack of portability. Whilst portable or bench top Raman microscopes are available for field applications of MRS,<sup>11</sup> the system still requires optical alignment expertise to collect the Raman signal. A true portable MRS system should be completely alignment-free and should be able to record Raman spectra in daylight.

It is worth noting that other spectroscopic methods when implemented in microfluidics have moved from a free space, bulk optic geometry to embedded fiber based geometries to achieve miniaturization and portability of the system.<sup>12</sup> For example, in

SUPA, School of Physics and Astronomy, University of St Andrews, North Haugh, Fife, KY16 9SS, UK. E-mail: pca7@st-andrews.ac.uk

† Published as part of a LOC themed issue dedicated to UK Research: Guest Editors Professors Hywel Morgan and Andrew deMello.

order to achieve fiber based fluorescence or absorption spectroscopy on a microfluidic platform, an optical fiber may be embedded into the microfluidic chip, with a predefined fiber insertion channel, in such a way that the tip of the fiber is separated from the fluidic channel by a wall of thickness in the order of 100  $\mu\text{m}$ .<sup>13,14</sup> However, for the successful implementation of Raman spectroscopy in microfluidics, this approach is not feasible as it does not ensure the maximum signal collection and fails to eliminate the substrate background as the excitation beam has to pass through the substrate.

We have previously reported the implementation of an MRS device, which was one of the attempts towards such a fiber based Raman detection system in a microfluidic platform, where a split Raman probe was embedded into a PDMS based fluidic chip.<sup>10</sup> Even though this system was alignment-free, the Etendue mismatch at the probe head limited the collection efficiency of the device. More importantly the dimension of the fluidic channel could not be reduced beyond the order of millimetres. The lack of scalability in terms of the fluidic channel size limited its applications and did not render it a good candidate for an ideal fiber based MRS system as it is practically impossible to integrate any microfluidic functionalities into this device.

In this article we propose the use of Waveguide Confined Raman Spectroscopy (WCRS) which can be considered as an ideal technology for achieving fiber based MRS. This technology offers scalability and efficient Raman signal collection without any background from the substrate in an alignment-free architecture. The basic idea behind this approach is to use a pair of embedded waveguides in the microfluidic channel to excite and collect the Raman signal. In this configuration, the end of the waveguide in the signal collection region contains no optical elements which would modify the output beam profile from the waveguide. Also the relative distance between the end of excitation and collection waveguides would be in the order of the size of the core of the waveguides. This would result in a confined excitation and collection of the Raman signal from close vicinity of the ends of the waveguides, maximizing the collection efficiency of the Raman signal. Also this approach ensures elimination of any background from the substrate. A notable feature of this detection scheme is its alignment-free nature due to the embedded waveguides. Hence WCRS can be used for analyte detection with minimal sample preparation requirements.

We demonstrate WCRS using a pair of embedded multimode optical fibers in a PDMS based microfluidic chip as shown in Fig. 1a. The effects of various device parameters to the performance characteristics of the device were investigated and optimized. Further the sensitivity of the device was estimated to compare its performance to the fiber probe based counterpart.<sup>10</sup>

In order to implement WCRS, it is possible to choose the fiber with the desired cladding size depending on the size of the microfluidic channels. Thus WCRS may be implemented in a variety of microfluidic functional devices. In order to demonstrate its compatibility with other microfluidic architectures, two functional microfluidic devices have been implemented, where WCRS was used for *in situ* probing of samples. The first device was a microreactor where a binary chemical reaction was monitored using WCRS.

The second device was a microdroplet based microfluidic system. Microdroplet based microfluidic systems are preferred

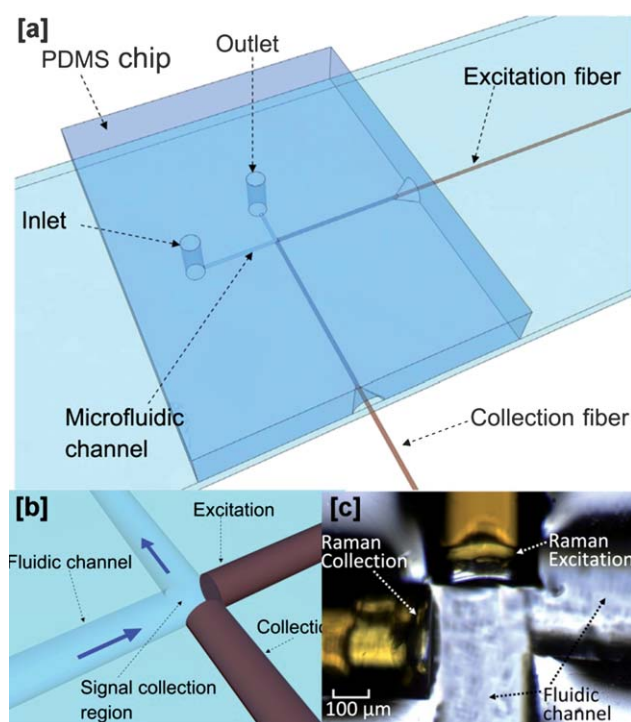


**Fig. 1** [a] Schematic of the PDMS microfluidic chip where WCRS was implemented. [b] Schematic diagram of the WCRS signal collection region where confined collection of Raman signal was achieved. [c] Top view of the Raman signal collection region in the PDMS microfluidic chip.

for bio-chemical reactions and analysis as the compartmentalization provides the advantage of keeping the reactants or the sample isolated. Microdroplets are of interest for biologists, as it is possible to mimic a cell like system within a microdroplet for genomics, proteomics or system biology studies.<sup>15</sup> Raman spectroscopy has already been used within a microfluidic platform for probing a sample encapsulated in microdroplets<sup>16–19</sup> using bulk optic Raman systems. Here we used WCRS for probing a microdroplet of ethanol generated in a buffer of silicone oil.

The fiber based Raman detection realized in microfluidics through WCRS could be an important step forward in the field of MRS. WCRS would enable rapid analyte detection with a reduction of the required sample volume.

## Experimental

### Embedding fiber into a microfluidic chip

The microfluidic chip was fabricated using soft lithography in PDMS.<sup>20</sup> In order to embed the optical fiber into the chip, fiber insertion channels had to be defined in the mould for the microfluidic chip. The fabrication procedure of the mould with pre-defined fiber insertion channel is explained in detail by Ashok *et al.*<sup>21</sup> The fiber insertion channels were defined by placing pieces of fibers on the silicon substrate, on which the mould was fabricated, and by fixing it using UV curable adhesive (Norland). The size of the fluidic channel near the detection region also depends on the diameter of the optical fiber including the cladding. Commercially multimode optical fibers are available in a range of diameters from 125  $\mu\text{m}$  to 250  $\mu\text{m}$ . We used

a negative photoresist (SU8, Microchem) to define other microfluidic channels. In order to combine the channels defined by the fiber to the channel defined by photoresist, the photoresist was spun on top of the silicon substrate to which the fiber pieces are already attached. Using photolithography, SU8 channels were defined on the substrate in such a way that the SU8 channel would physically be connected to the fiber which is stuck on the mould.

Once the mould was prepared, the PDMS chip was fabricated using soft lithography and the excitation and collection fibers were inserted into the chip as shown in Fig. 1a. Since the fiber insertion channel was predefined for the desired collection geometry, the alignment requirement was minimal while inserting the fiber into the channel as shown in Fig. 1b and c.

### Raman detection system

The Raman signal was excited and collected using low OH multimode fibers. For all the experiments discussed in this paper, except those to study the effect of core size on collection efficiency, a multimode fiber with core size 200  $\mu\text{m}$  (Polymicro Technologies, Arizona, USA) was used. We used a laser of wavelength 785 nm (Laser2000 (UK) Ltd., maximum power  $\sim 450$  mW) for Raman excitation. The laser was coupled into the optical fiber through an SMA connector and the other end of the fiber was embedded into the microfluidic chip for Raman excitation. The tip of the collection fiber, which was embedded into the microfluidic chip, collected the Raman signal which was then coupled to the spectrometer (Shamrock SR-303i, Andor Technology) through a telescopic system to match the F-number of the fiber to that of the spectrometer. A long-pass filter (cut-off wavelength 795.2 nm, Semrock, Inc. USA) was incorporated between the two lenses of the telescope to filter out the Rayleigh scattered photons. The spectrometer employed a 400 lines per mm grating and was equipped with a deep depletion, back-illuminated and thermoelectrically cooled CCD camera (Newton, Andor Technology) for the detection of Raman signal. With a slit width of 150  $\mu\text{m}$ , the resolution of the Raman system was measured by the FWHM of the ethanol peak at 884  $\text{cm}^{-1}$  and was found to be better than 14  $\text{cm}^{-1}$ . Since we used the same Raman detection system, the external appearance of the WCRS based microfluidic detection system would be same as that in our previously reported work.<sup>10</sup>

### Characterization of the device

In order to investigate the performance parameter of the device, ethanol (Sigma Aldrich) was taken as a model analyte. The effects of three parameters—length, relative angle and core size of excitation and collection fibers—on the collection efficiency of Raman signal and fluorescence background were studied. For these observations, the power of the laser was fixed at 200 mW. For each data point, 20 Raman spectra of ethanol were collected with an acquisition time of 2 s for each spectra.

The effect of the length of the fiber was studied by reducing the fiber length using a cut back method, keeping all other parameters constant. In order to study the effect of angle, a microfluidic chip with fiber insertion channels at different relative angles was fabricated and Raman signal of ethanol was collected keeping all

other parameters constant. In order to study the effect of core sizes three low OH multimode fibers with core sizes 50  $\mu\text{m}$ , 105  $\mu\text{m}$  (Thorlabs Inc., USA) and 200  $\mu\text{m}$  were used. Depending on the size of the cladding a microfluidic chip with suitable size of fiber insertion channels was fabricated. Since fibers with 50  $\mu\text{m}$  and 105  $\mu\text{m}$  had the same cladding size (125  $\mu\text{m}$ ), the collection efficiency was estimated for different combinations of these two fibers for excitation and collection.

In order to estimate the minimum detection limit of the device for detecting the urea, Raman spectra of urea at different concentrations were collected for an acquisition time of 5 s each and the laser excitation power was 200 mW.

### Monitoring of microreaction in a microreactor

In order to demonstrate the ability to use WCRS for process monitoring, WCRS was incorporated into a microreactor as shown in Fig. 2. The serpentine microreactor was designed for a binary reaction where the serpentine consisted of a microfluidic channel of rectangular cross-section with 150  $\mu\text{m}$  width and 60  $\mu\text{m}$  height. The serpentine region was then widened into a microfluidic channel with circular cross-section with a diameter of 250  $\mu\text{m}$ , where the multimode fibers were embedded for WCRS detection. The total volume of the mixing region, from the junction where reactants begin mixing to the WCRS detection region, was 8.83  $\mu\text{l}$ .

The acid catalyzed esterification of ethanol with acetic anhydride to produce ethyl acetate was chosen as the model reaction to be monitored using WCRS. Sulfuric acid was used as the catalyst for the reaction, a minute amount of which was added into the reactants prior to the reaction. All the reagents used (Sigma Aldrich) were of analytical quality. The reaction was carried out at room temperature  $\sim 22$   $^{\circ}\text{C}$ . The solutions were pumped into the microreactor using syringe pumps (Harvard Apparatus). The stoichiometric ratio of acetic anhydride to ethanol was 1 : 2 for this reaction, which would be 1 : 3.24 in

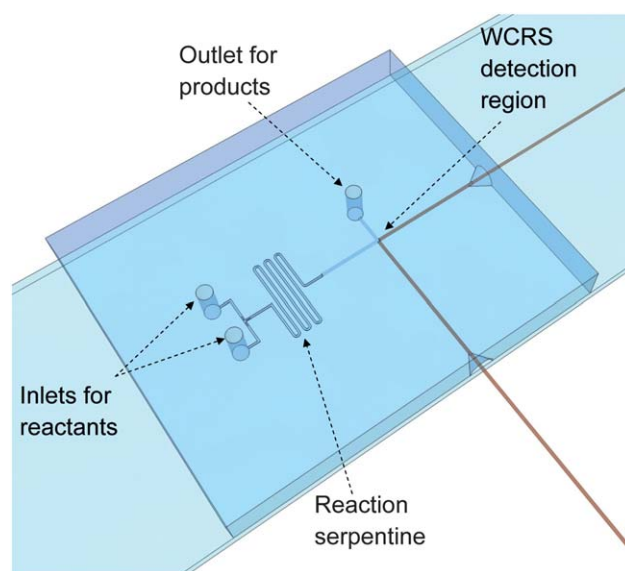


**Fig. 2** Design of the WCRS incorporated microreactor chip (only a representative drawing of the serpentine region is shown; in the actual microfluidic chip, the serpentine region is longer).

volume. The ratio of the flow rates of the reactants was fixed to be 1 : 4 since ethanol was the carrier solvent. The dynamics of the chemical reaction was studied at different analyte flow rates whose results are discussed later.

### Generation and WCRS detection of microdroplets

The use of microdroplet based microfluidic systems has proved useful for various microfluidic applications. In contrast to bulk techniques, microfluidics lends itself well to the creation of sample-in-oil emulsions with controlled droplet sizes.<sup>15</sup> We combined a microdroplet generation design with WCRS to show the capability of WCRS to probe the sample in the microdroplet as shown in Fig. 3a. There are two popular geometries for the creation of these nanolitre sized droplets: the 'T-junction'<sup>22</sup> and 'flow focusing'.<sup>23</sup> We opted for a simple T-junction design where the sample and oil buffer meet at right angles for the droplet formation as shown in Fig. 3b. When the two immiscible phases meet at the junction, the oil flow exerts a shearing force on the sample flow, which causes it to break into discrete microdroplets. By adjusting the relative flows of the two immiscible phases, droplets of various sizes can be formed on a single microfluidic chip<sup>24</sup> as shown in Fig. 3c.

The droplet generation region in the microfluidic chip had a rectangular cross-section with a width of 100  $\mu\text{m}$  and a height of 50  $\mu\text{m}$ . Further downstream, the microfluidic channel widened into a channel with a circular cross-section of diameter 250  $\mu\text{m}$ , where the Raman spectra were collected. Ethanol, diluted to 50% using de-ionised water, was used as the sample. Droplets of ethanol were created within a continuous phase of silicone oil (Sigma Aldrich) containing Span 85 (Fluka) surfactant mixed at a volume ratio of 9.7 : 0.3.<sup>25</sup>

Droplets were imaged using a high speed camera (Fastec Troubleshooter, Fastec Imaging) at 250 frames per second at

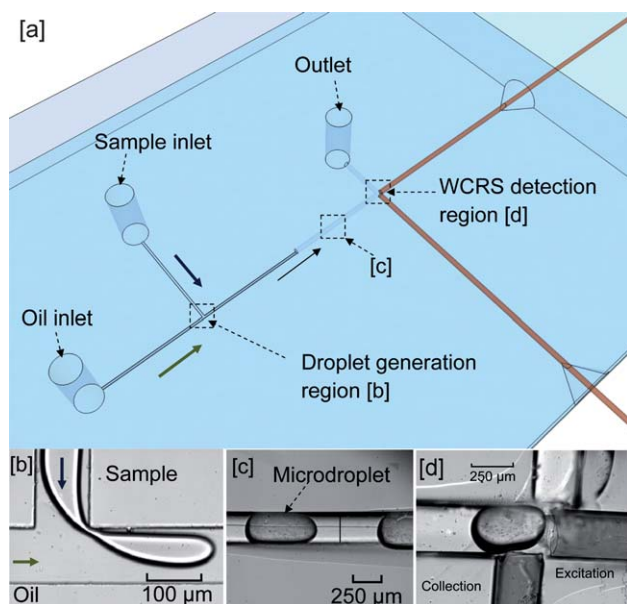


**Fig. 3** [a] Design of the microfluidic chip for microdroplet generation combined with WCRS. [b] Microdroplet generation region. [c] Microdroplet flowing through the microfluidic channel. [d] WCRS detection of microdroplets.

three regions of interest: the T-junction, downstream and at the Raman detection region (Fig. 3b, c and d respectively). The droplet volume was calculated by approximating its shape within the round channel to a cylinder and two partial ellipsoids representing the curved 'head' and 'tail'. At a flow ratio of 1 : 1 and flow rates of 120  $\mu\text{l h}^{-1}$ , the droplet volume was  $\sim 18.5$  nl. Raman spectra were collected using WCRS for an acquisition time of 1 s which corresponds to 1.8 droplets passing through the detection region during one acquisition.

### Results and discussion

WCRS is based on two concepts of confinements. The first confinement is of the Raman signal collection. The output from the optical fiber diverges at an angle 12.7°. For a length <200  $\mu\text{m}$ , the beam size is comparable to the size of the core, beyond which the power density drops down significantly. Hence it is important to collect the Raman signal from a region close to the apex of the excitation fiber, and the same logic applies for the collection fiber for maximum collection efficiency. Fig. 4a shows how the maximum overlap of excitation and collection is achieved by collecting the signal right from the apex of the fiber.

The second aspect of confinement is in terms of the sample. The microfluidic channel, which has similar size as that of the excitation and collection waveguide, can confine the sample to be interrogated within the confined signal collection region. One of the advantages of this approach is that no other part of the microfluidic channel, or substrate overlaps with the collection volume; hence there would not be any spurious background from the substrate in the Raman spectra acquired using WCRS. Also, since channel size is in the order of 125–250  $\mu\text{m}$ , the required amount of sample volume is five orders lower than that of its probe based counterpart as shown in Fig. 4b. It is important to note that a further reduction in the channel size is possible if instead of optical fibers, on-chip integrated waveguides of smaller dimensions were fabricated for Raman signal collection.

In WCRS, since a diverging beam is used for excitation, the whole cross-section of the microfluidic channel is being interrogated, in contrast to other systems where a focused beam achieves only partial interrogation of the channel cross-section.<sup>26</sup> Hence in WCRS, the required sample volume is completely interrogated in contrast to microscope based or probe based MRS systems where the required sample volume would be greater than the probed sampling volume. Since the volume of interrogation is larger, the overall power density seen by the analyte is lower for WCRS based detection. Hence in WCRS,

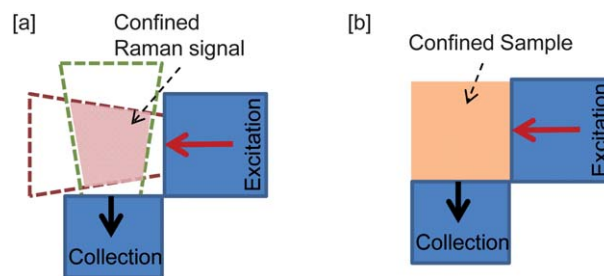


**Fig. 4** [a] 2D projection of the WCRS detection area, showing the Raman signal collection area. [b] 2D projection of the WCRS detection area showing the confinement of the sample.

a higher power could be used, keeping a low power density, thereby reducing the required acquisition time compared to confocal systems.

Since sensitive detectors are used for Raman spectroscopy, Raman measurements in broad daylight are difficult due to the background from the ambient light. The form factor of conventional Raman microscopes makes it difficult to be darkened for field applications where Raman measurements have to be performed in broad daylight. Since WCRS has confined signal collection, where *in situ* probing of the microfluidic channel is performed, and the Raman signal is delivered into the spectrometer through an optical fiber, only the microfluidic chip has to be kept in darkness for Raman measurements in daylight, making it more amenable for field applications.

### Effect of angle of collection

The collection efficiency and fluorescent background depend strongly on the angle of collection. The effect of the relative angle between the excitation and collection fibers was studied using the ethanol peak at  $884\text{ cm}^{-1}$  as the reference peak. As shown in Fig. 5a, baselining was performed on the raw Raman spectra of ethanol. For the region between  $870\text{ cm}^{-1}$  and  $900\text{ cm}^{-1}$ , the area under the baseline was considered to be fluorescent background and the area above the baseline was considered to be Raman signal. Fig. 5 shows the variation of peak intensity and fluorescent background for different angles of collection.

At obtuse angles of collection, the collection fiber collects more fluorescent background and forward scattered photons from the excitation fiber. These forward scattered photons, entering into the collection fiber, generate further fluorescence background. This explains the decrease in the ratio of Raman signal to the fluorescent background for collection angles  $>90^\circ$  and saturation of the detector when collection angle was  $>120^\circ$ .

At acute collection angles, with the decrease in collection angle the collection volume, which is the overlap volume of the output beam profile cones of excitation and collection fibers, moves away from the apex of the excitation and collection fibers. This results in a shift of collection volume towards the periphery of the beam profile cones leading to a reduced number of Raman excitation photons within the collection volume. Hence it can be seen that as the collection angle decreases, the total intensity of the signal decreases, even though the variation in the ratio of Raman signal to fluorescent background is minimal.

The optimum collection angle was found to be  $90^\circ$  where the total signal strength and the ratio of Raman signal to the fluorescent background were maximum.

### Effect of length of the fiber

Since fibers were used for excitation and collection, and no filters were used at the apex of the fiber, there could be fluorescence contributions from the fiber in the detected Raman spectra. The effect of the length of the fiber on the Raman spectra was studied by varying the length of excitation and collection fibers. The ethanol Raman peak at  $884\text{ cm}^{-1}$  was used as the reference peak and an analysis, similar to that mentioned for Fig. 5, was used. The results are shown in Fig. 6.

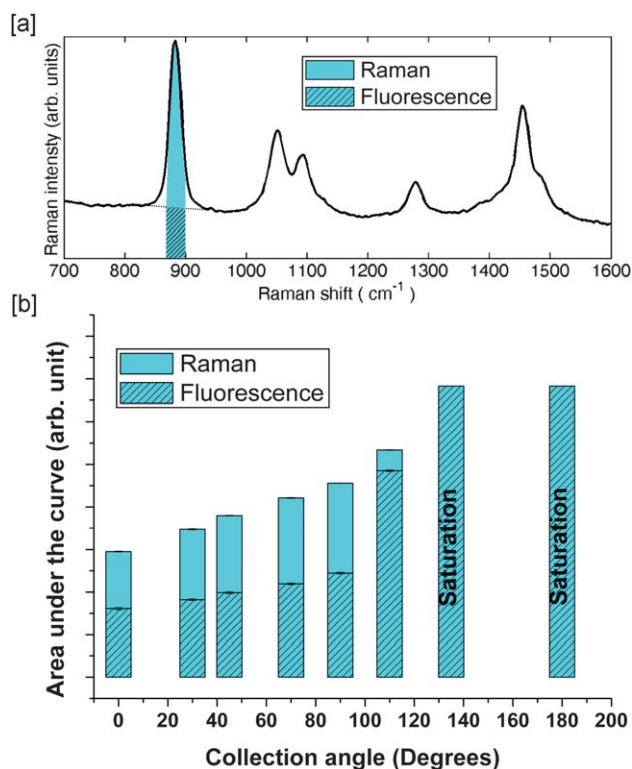


**Fig. 5** [a] Raw Raman spectra of ethanol recorded in the orthogonal WCRS geometry in order to show the estimation of the level of fluorescence and Raman signal. The area under the shaded region was used for the estimation of fluorescent and Raman signals. [b] Area under the Raman peak of  $884\text{ cm}^{-1}$  of the Raman spectrum of ethanol for different collection angles. Each data point is an average of 20 Raman spectra, recorded with an acquisition time of 2 s each and the error bar is the standard deviation of 20 spectra (error bars not visible as it is two orders of magnitude lower than that of the average value).

It can be seen that the fluorescence background does not vary with the length of the fiber. This is due to the fact that, in the orthogonal geometry, the majority of the fluorescence background coming from the excitation fiber would not be collected by the collection fiber. Also in this collection geometry, the minimum amount of Rayleigh scattered excitation photons would be collected by the collection fiber, so that the fluorescence excited in the collection fiber would be minimized. Hence in the orthogonal collection geometry, the length of excitation and collection fibers does not affect the WCRS signal.

### Effect of core size of the fiber

As mentioned in the Introduction, WCRS is a scalable technique. It is possible to choose a waveguide of a suitable size, depending on the dimensions of the microfluidic channels. However the collection efficiency could be affected when the core size of the fiber is varied. The effect of core size is studied by collecting the Raman spectra of ethanol using low OH multimode fibers of different core sizes keeping the power of excitation constant, the result of which is shown in Fig. 7.

It can be seen that the collection efficiency is mainly affected by the parameters of the collection fiber. There is no variation in the

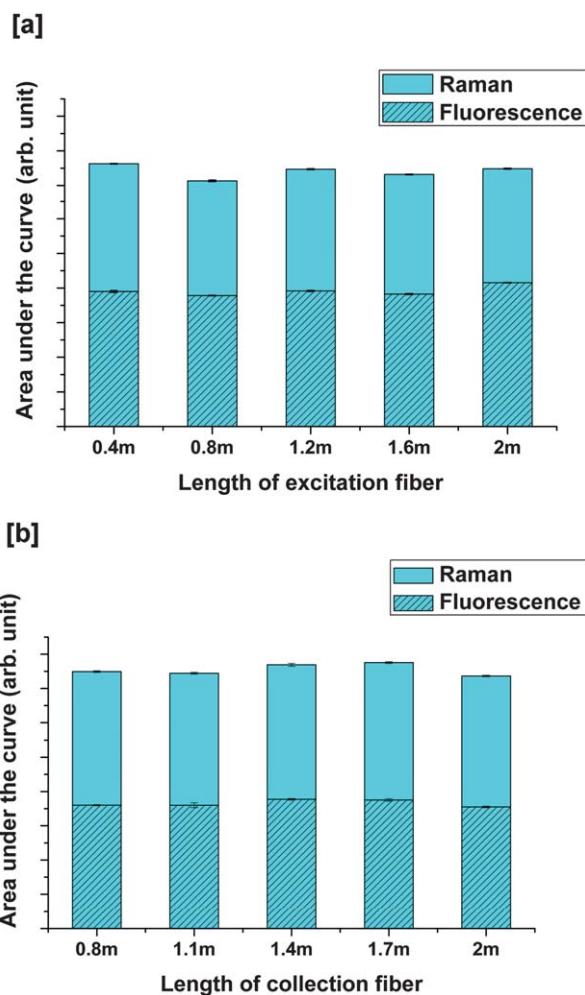


**Fig. 6** Area under the ethanol Raman peak of  $884\text{ cm}^{-1}$  for varying length of excitation fiber [a] and collection fiber [b]. In [a] the collection fiber length was fixed at 1 m and in [b] the excitation fiber length was fixed at 1 m. Each data point is an average of 20 Raman spectra, recorded with an acquisition time of 2 s and the error bar is the standard deviation of 20 spectra (error bars not visible as it is two orders of magnitude lower than that of the average value).

collection efficiency when the core size of the excitation fiber was varied, keeping the core size of the collection fiber constant. Also it can be seen that the collection efficiency is comparable for a 200  $\mu\text{m}$  (250  $\mu\text{m}$  cladding diameter) core size fiber and a 100  $\mu\text{m}$  (125  $\mu\text{m}$  cladding diameter) core size fiber. This proves that WCRS is a scalable technique and may be adapted to a range of microfluidic dimensions.

#### Minimum detection limit for urea

In order to compare the performance of WCRS to its fiber probe counterpart,<sup>10</sup> the minimum detection limit of urea was calculated using WCRS in similar experimental conditions. The Noise Equivalent Concentration (NEC)<sup>10</sup> was estimated to be 80 mM as shown in Fig. 8, which is better than the probe based system.

Even though there are filters at the probe head of the probe based system, there would be an insertion loss at the probe head due to the throughput (Etendue) mismatch between the probe head and the collection fiber, which would result in the reduction

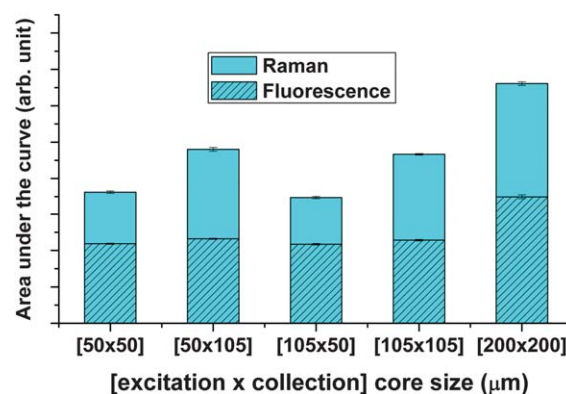


**Fig. 7** Area under the peak of  $884\text{ cm}^{-1}$  of the Raman spectra of ethanol for different core sizes for excitation and collection each data point is an average of 20 Raman spectra, recorded with an acquisition time of 2 s and the error bar is the standard deviation of 20 spectra. (Error bars not visible as it is two orders of magnitude lower than that of the average value).

of the sensitivity of the system. There is a tradeoff between the net collection efficiency of the system and fluorescent background. In WCRS, the absence of filters at the tip of the fiber would result in increased fluorescent background. However, since the Raman signal is being collected directly to the collection fiber, there is no throughput mismatch. It can be seen from the NEC calculation that even though the fluorescent background is higher, the minimum detection limit is better for WCRS when compared to a probe based system. Also the required sample volume is five orders lower for WCRS when compared to its probe based counterpart because of the smaller channel dimensions.

#### Process monitoring using WCRS

There are various reported studies where a microreaction in a microreactor was monitored using Raman spectroscopy.<sup>9</sup> Spatial and temporal mapping of the progress of reaction was

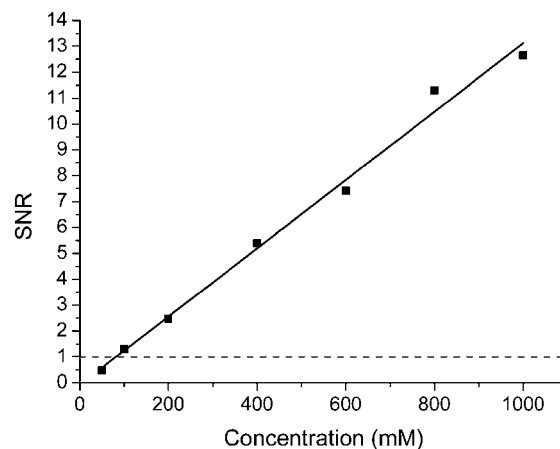


**Fig. 8** Plot of concentration vs. SNR for Raman spectra of urea. The '■' represents the SNR measured at a particular concentration from 10 spectra recorded with 5 s acquisition time each. The solid line represents the linear fit for the evaluated SNR data. The dotted line represents the limit of detection where  $\text{SNR} = 1$ . The Noise Equivalent Concentration (NEC) is evaluated as 80 mM from the plot.

achieved in such studies.<sup>4,6</sup> However in all these studies, the Raman system probed the microfluidic channel from outside the microfluidic chip, resulting in a reduced sensitivity, higher acquisition time and significant background from the substrate. Also the quality of the Raman spectra obtained largely depends on the alignment of the interrogating optics with respect to the microfluidic channel.<sup>6</sup>

WCRS offers a solution to all these problems, resulting in high sensitive, fast, background-free and alignment-free acquisition of Raman spectra in a microreactor. Even though it is not possible to achieve spatial mapping of the fluidic channel using WCRS, it is possible to study the reaction dynamics by varying the flow rates of the analytes and can obtain similar information as obtained through spatial mapping using a free space system.<sup>6</sup>

We studied the progress of reaction at different interaction time scales for a binary reaction. By changing the total flow speed, the interaction time for the two reactants was varied. Interaction time was the time duration for the analyte to flow from the “T” junction where the analytes were combined to the WCRS detection region. Prior to the actual experiment, the pure spectra of the reactants (acetic anhydride and ethanol) and product (ethyl acetate) were obtained using WCRS and compared with the spectra of analyte for an incomplete reaction as shown in Fig. 9a. Since the product analyte had an incomplete reaction, the Raman peaks corresponding to all reactants and products could be seen. The Raman spectra shown in Fig. 9a were smoothed using a Savitzky–Golay smoothing filter and baselined using iterative modified polynomial fitting.<sup>27</sup> From the spectra it is clear that the Raman peak at  $671\text{ cm}^{-1}$  for acetic anhydride and the Raman peak at  $636\text{ cm}^{-1}$  for ethyl acetate would be two representative peaks to be monitored to study the progress of the chemical reaction in the microreactor. The concentration of ethanol was not monitored as it was the carrier solvent.

The total flow rate of the analyte was varied in order to change the interaction time of the reactants. Raman spectra of the analyte were obtained using WCRS with an acquisition time of 2 s. Fig. 9b shows the variation in the concentration of ethyl acetate and acetic anhydride with respect to the change in flow rate. Each data point is an average of 40 Raman spectra. Savitzky–Golay smoothing was performed on the Raman spectra as a post-processing step before estimating the peak intensity value. We observed that, at low flow rates, the reaction completed within the interaction time and the peaks corresponding to acetic anhydride were missing from the recorded Raman spectra. However for higher flow rates the reaction was incomplete so that the acetic anhydride peak was visible in the Raman spectra and the intensity of the peak corresponding to ethyl acetate decreased. The recorded spectra were completely free from any background from the substrate of the microfluidic chip and also there was no requirement for any optical alignment during the experiment. This shows that WCRS is a powerful Raman spectroscopic based detection scheme for process monitoring and to study the dynamics of a reaction in a microreactor based microfluidic chip.

### Detection of microdroplets using WCRS

As mentioned in the Introduction, Raman spectroscopy has been used to probe microdroplets from outside of the chip using

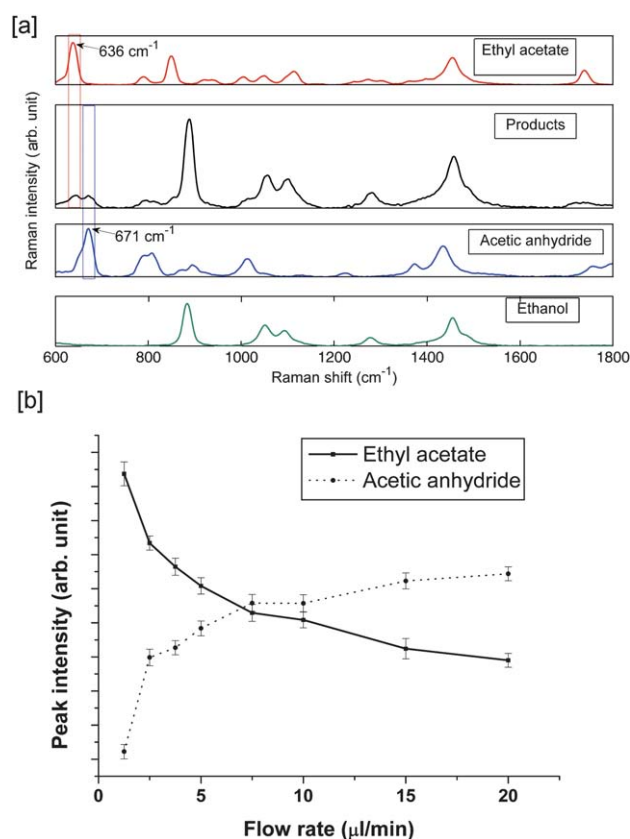


**Fig. 9** [a] Comparison of the pure Raman spectra of the reactants and products with the Raman spectra of an analyte where the reaction was partially completed. [b] Variation of the Raman peak intensity of ethyl acetate at  $636\text{ cm}^{-1}$  and that of acetic anhydride at  $671\text{ cm}^{-1}$  for different interaction times of the reactants in the microreactor serpentine. Each data point is an average of 40 Raman spectra, recorded with an acquisition time of 2 s and the error bar is the standard deviation of 40 spectra.

confocal<sup>17,19</sup> and non-confocal<sup>16</sup> approaches. The acquisition times in these studies range from 10 s to a few minutes in order to get the fingerprint of the sample inside the microdroplet. Several microdroplets would pass through the Raman collection region during this comparatively long acquisition time. Meanwhile the oil phase also passes through the collection region, so that the collected spectra would have signatures of the sample and the oil buffer. It is possible to monitor the analyte inside the microdroplet by looking into the Raman peaks that are not interfering with those of the oil. However with a longer acquisition time, the Raman spectra collected would be an average of the signal from several microdroplets (10 s to 100 s) thereby reducing the spatial resolution of the detection scheme.

We used WCRS for probing the analyte inside a microdroplet. Since WCRS has higher sampling volume compared to confocal systems, it would be possible to reduce the net acquisition time. As a proof of principle, we generated a microdroplet of a diluted ethanol (40%) sample and collected Raman spectra of it using WCRS. Fig. 10 shows the Raman spectra collected in a microdroplet generation channel with an acquisition time of 1 s and compares it with those of the pure spectra of oil and ethanol. The spectra were smoothed using a Savitzky–Golay polynomial and baselined.

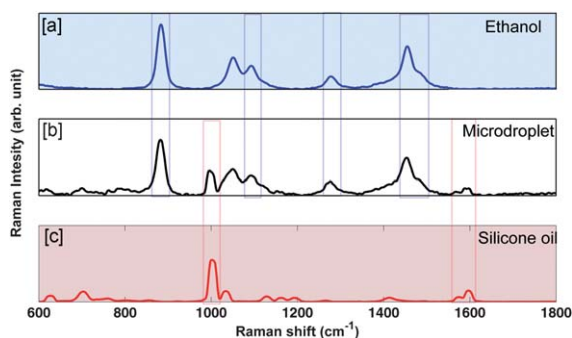


**Fig. 10** [b] Raman spectra collected using WCRS from a microdroplet system containing ethanol as sample with an acquisition time of 1 s. [a and c] Pure Raman spectra of ethanol and silicone oil.

It can be seen that the major peaks in the Raman spectra of ethanol are clearly visible in the spectra along with the peaks for oil. For the flow rates we used, during a period of 1 s, 1.8 droplets would pass through the Raman analysis region. The strong Raman peaks of ethanol, shown in Fig. 10 suggest that it is possible to reduce the acquisition time further down. Hence, in principle it would be possible to use WCRS for probing a single droplet in a microdroplet based microfluidic system. The possibility of probing a single microdroplet using Raman spectroscopy would open opportunities for studying microdroplet dynamics at an enhanced temporal resolution. This can also lead to the realization of Raman activated microdroplet sorting devices.

## Conclusion

WCRS is a novel Raman detection technique which enables fiber based Raman detection in microfluidics using on-chip embedded waveguides. This approach is scalable and easily adaptable to various microfluidic architectures and allows to achieve alignment-free and fast acquisition of Raman spectra of analytes without any background from the substrate of the microfluidic chip. Also the divergent beam used for Raman excitation allows us to maximize the sampling volume in the microfluidic channel. The performance characteristics of WCRS have been investigated for various parameters. It has been found that the orthogonal collection geometry gives maximum collection efficiency with minimum fluorescent background. The fluorescence background in the recorded spectra is independent of the length of the excitation and collection fiber. Also the collection efficiency is mainly dependent on the core size of the collection fiber.

As a device, WCRS can be used for sensitive analyte detection with minimal sample preparation. The minimum detection limit of this device to detect urea was estimated to be 80 mM for an acquisition time of 5 s with 200 mW excitation power which is better than its probe based counterpart.<sup>10</sup> This would pave the way to develop sensitive and portable bioanalyte detection devices using Raman spectroscopy that can be used for detection with minimal sample preparation requirements. Another important feature of WCRS is that it could easily be combined with other microfluidic functionalities. As a proof of principle, we implemented WCRS in two microfluidic applications. We used WCRS for process monitoring in a microreactor and

showed that the reaction dynamics could be studied through Raman spectroscopy. Also WCRS has been used to probe microdroplets in a microdroplet based microfluidic system. We were able to obtain the Raman signature of the sample in the microdroplet with a very low acquisition time which could lead to development of Raman activated microdroplet sorting devices.

WCRS is a generic technique which is easily adaptable to various microfluidic platforms, so that the field of microfluidics could exploit the advantages of Raman spectroscopy. WCRS may result in the development of efficient, alignment-free, portable MRS devices for sensing and process monitoring that are suitable for field applications. With WCRS, it is now possible to translate many of the MRS devices, implemented in a bulk optic geometry into a fiber based alignment-free geometry. It is possible to implement variants of Raman spectroscopy such as SERS, resonance Raman spectroscopy in WCRS for extending its applicability. Further exploration is necessary for biological applications of WCRS based microfluidic devices. Portable microfluidic devices with Raman spectroscopic detection, realized through WCRS, may have applications in point of care disease diagnosis, drug development, pharmaceutical manufacturing, cell biology, proteomics and environmental sensing.

## Acknowledgements

We acknowledge the Cancer Research UK and the Engineering and Physical Sciences Research Council (EPSRC), in association with the Medical Research Council (MRC) for funding. We also thank the EU FP7 STREP programme “Araknes” for funding. KD is a Royal Society-Wolfson Merit Award Holder. The authors are grateful to Dr Andrew McKinley for the discussions about the chemical reaction used for the microreactor experiments.

## References

- H. C. Hunt and J. S. Wilkinson, *Microfluid. Nanofluid.*, 2008, **4**, 53–79.
- P. A. Walker, M. D. Morris, M. A. Burns and B. N. Johnson, *Anal. Chem.*, 1998, **70**, 3766–3769.
- O. Svensson, M. Josefson and F. W. Langkilde, *Chemom. Intell. Lab. Syst.*, 1999, **49**, 49–66.
- P. D. I. Fletcher, S. J. Haswell and X. L. Zhang, *Electrophoresis*, 2003, **24**, 3239–3245.
- M. Lee, J. P. Lee, H. Rhee, J. Choo, Y. G. Chai and E. K. Lee, *J. Raman Spectrosc.*, 2003, **34**, 737–742.
- S. Mozharov, A. Nordon, J. M. Girkin and D. Littlejohn, *Lab Chip*, 2010, **10**, 2101–2107.
- J. B. Salmon, A. Ajdari, P. Tabeling, L. Servant, D. Talaga and M. Joanicot, *Appl. Phys. Lett.*, 2005, **86**, 094106.
- S. A. Leung, R. F. Winkle, R. C. R. Wootton and A. J. deMello, *Analyst*, 2005, **130**, 46–51.
- P. J. Viskari and J. P. Landers, *Electrophoresis*, 2006, **27**, 1797–1810.
- P. C. Ashok, G. P. Singh, K. M. Tan and K. Dholakia, *Opt. Express*, 2010, **18**, 7642–7649.
- L. X. Quang, C. Lim, G. H. Seong, J. Choo, K. J. Do and S. K. Yoo, *Lab Chip*, 2008, **8**, 2214–2219.
- S. Gotz and U. Karst, *Anal. Bioanal. Chem.*, 2007, **387**, 183–192.
- H. F. Li, J. M. Lin, R. G. Su, K. Uchiyama and T. Hobo, *Electrophoresis*, 2004, **25**, 1907–1915.
- B. Ibarlucea, E. Fernandez-Rosas, J. Vila-Planas, S. Demming, C. Nogues, J. A. Plaza, S. Büttgenbach and A. Llobera, *Anal. Chem.*, 2010, **82**, 4246–4251.

- 15 A. Huebner, S. Sharma, M. Srisa-Art, F. Hollfelder, J. B. Edel and A. J. Demello, *Lab Chip*, 2008, **8**, 1244–1254.
- 16 S. E. Barnes, Z. T. Cygan, J. K. Yates, K. L. Beers and E. J. Amis, *Analyst*, 2006, **131**, 1027–1033.
- 17 G. Cristobal, L. Arbouet, F. Sarrazin, D. Talaga, J. L. Bruneel, M. Joanicot and L. Servant, *Lab Chip*, 2006, **6**, 1140–1146.
- 18 K. R. Strehle, D. Cialla, P. Rosch, T. Henkel, M. Kohler and J. Popp, *Anal. Chem.*, 2007, **79**, 1542–1547.
- 19 F. Sarrazin, J. B. Salmon, D. Talaga and L. Servant, *Anal. Chem.*, 2008, **80**, 1689–1695.
- 20 J. C. McDonald, D. C. Duffy, J. R. Anderson, D. T. Chiu, H. Wu, O. J. A. Schueller and G. M. Whitesides, *Electrophoresis*, 2000, **21**, 27–40.
- 21 P. C. Ashok, R. F. Marchington, P. Mthunzi, T. F. Krauss and K. Dholakia, *Opt. Express*, 2010, **18**, 6396–6407.
- 22 T. Thorsen, R. W. Roberts, F. H. Arnold and S. R. Quake, *Phys. Rev. Lett.*, 2001, **86**, 4163–4166.
- 23 S. L. Anna, N. Bontoux and H. A. Stone, *Appl. Phys. Lett.*, 2003, **82**, 364–366.
- 24 P. Garstecki, M. J. Fuerstman, H. A. Stone and G. M. Whitesides, *Lab Chip*, 2006, **6**, 437–446.
- 25 M. Y. He, J. S. Edgar, G. D. M. Jeffries, R. M. Lorenz, J. P. Shelby and D. T. Chiu, *Anal. Chem.*, 2005, **77**, 1539–1544.
- 26 R. M. Connatser, L. A. Riddle and M. J. Sepaniak, *J. Sep. Sci.*, 2004, **27**, 1545–1550.
- 27 C. A. Lieber and A. Mahadevan-Jansen, *Appl. Spectrosc.*, 2003, **57**, 1363–1367.